Materials Science and Engineering A 530 (2011) 607–617

Contents lists available at SciVerse ScienceDirect

Materials Science and Engineering A

journal homepage: www.elsevier.com/locate/msea

Effect of solution treatment on precipitation behaviors and age hardening response of Al–Cu alloys with Sc addition

B.A. Chen[a], L. Pan[a], R.H. Wang[b], G. Liu[a,*], P.M. Cheng[a], L. Xiao[a], J. Sun[a,*]

[a] State Key Laboratory for Mechanical Behavior of Materials, Xi'an Jiaotong University, Xi'an 710049, China
[b] School of Materials Science and Engineering, Xi'an University of Technology, Xi'an 710048, China

ARTICLE INFO

Article history:
Received 1 May 2011
Received in revised form 10 August 2011
Accepted 6 October 2011
Available online 18 October 2011

Keywords:
Aluminum alloys
Precipitation hardening
Sc addition
Solution treatment

ABSTRACT

Influences of solution treatment on precipitation behaviors and age hardening response of Al–2.5 wt% Cu–0.3 wt% Sc alloys were investigated, in comparison with Sc-free one. The Al_3Sc dispersoids, formed during homogenization, were either survived or dissolved to become Sc solute atoms in solution treatment, depending on the solution temperature. When the temperature for solution treatment is 873 K, most of the Al_3Sc dispersoids were dissolved and a significant enhancement in the uniform precipitation of finer θ'-Al_2Cu particles was achieved in following aging treatment, causing a noticeable increase in peak-aging hardness by about 90% compared to Sc-free alloys. The enhanced age hardening effect was quantitatively related to the remarkable reduction in effective inter-particle spacing of the plate-shaped θ'-Al_2Cu precipitates. When the temperature for solution treatment is 793 K, however, most of the Al_3Sc dispersoids were survived after solution treatment and facilitated the heterogeneous precipitation of θ'-Al_2Cu plates directly on the {1 0 0} facets of dispersoids in following aging treatment. Concomitantly, the uniform precipitation of θ'-Al_2Cu plates was greatly suppressed, resulting in a reduced age hardening response. The age hardening responses were quantitatively assessed by using a modified strengthening model that is applicable to the plate-shaped precipitates. The calculations were in good agreement with experimental results. The present results show the importance of controlling solution treatments to achieve significant promotion effect of Sc addition on the precipitation hardening in heat-treatable aluminum alloys.

1. Introduction

The research on scandium (Sc) addition in aluminum (Al) alloys has been received increasing attention over the last decade, because of their interesting benefits. Most of the benefits are related to the formation of Al_3Sc particles, including Al_3Sc dispersoids and Al_3Sc precipitates [1]. Here, the Al_3Sc dispersoids are specially referred to the Al_3Sc particles formed in high temperature processing of the alloy, such as homogenization, hot-rolling or extrusion, while the Al_3Sc precipitates referred to those formed during aging process after solution treatment.

The well-known contribution of Al_3Sc dispersoids is to stabilize the grain/subgrain structure of Al alloys through Zener-drag action and hence enhance recrystallisation resistance [2–4]. Because of excellent thermal stability and high number density, the Al_3Sc dispersoids are very effective in preventing recrystallisation up to temperatures of about 350–400 °C [5]. By adding Sc and Zr in combination, the recrystallisation resistance of Al alloys can be further improved due to the formation of more stable core–shell $Al_3(Sc_xZr_{1-x})$ dispersoids [6–10]. The Al_3Sc precipitates, coherent with the Al matrix, can produce a significant strength increase in the Al alloys. It has been claimed [11,12] that Sc is a more effective precipitation hardening element per atomic fraction added than the element commonly used for precipitation hardening. However, the Al_3Sc precipitates that can be decomposed from supersaturated solid solution are rather limited, the absolute hardness/strength increase induced by precipitation hardening is relatively low [1].

The addition of Sc in pure aluminum or *non-heat-treatable* Al alloys (e.g., Al–Mn and Al–Mg alloys) has been extensively investigated [13–18], mainly due to two advantages. The first one is to strengthen these non-heat-treatable Al alloys by forming Al_3Sc precipitates, making them heat-treatable and creep-resistant. The second is to use Al_3Sc precipitates as model particles for studying basic principles in physical metallurgy, including coarsening behaviors [13–15] and interaction with dislocations [16–18]. In comparison, there have been much fewer studies on the Sc addition in *heat-treatable* Al alloys [19,20]. A major reason is that it is unfeasible for Sc addition to further strengthen the *heat-treatable* Al alloys by additionally forming Al_3Sc precipitates. The Al_3Sc precipitates

* Corresponding authors. Tel.: +86 29 82668610; fax: +86 29 82663453.
E-mail addresses: lgsammer@mail.xjtu.edu.cn (G. Liu), junsun@mail.xjtu.edu.cn (J. Sun).

0921-5093/$ – see front matter © 2011 Elsevier B.V. All rights reserved.
doi:10.1016/j.msea.2011.10.030

are hardly coexisted with other strengthening precipitates, because the temperature regime for aging treatment of Al_3Sc is between the temperature regimes for aging treatment and solution treatment of common heat-treatable Al alloys [1].

Effect of minor Sc addition on the precipitation behaviors and resultant aging response of *heat-treatable* Al alloys is far from clear. In some limited reports, contradictory information was presented: the Sc addition has been found to (i) improve [21,22], (ii) have no effect [23,24], or (iii) even suppress [25,26] the precipitation of other strengthening particles in heat-treatable Al alloys. No attempt has been made to explain the discrepancy in the reported effect of Sc addition. In this paper, we show through systematic investigations that the effect of Sc addition on the aging hardening of Al–Cu alloys is closely dependent on the existing forms of added Sc, which is modulated by the solution treatment.

Heat treatments of Al alloys are complicated by three steps of homogenization, solution, and aging. The last step of aging treatment is actually relied on the former two steps, and an appropriate cooperation of the three steps is required to achieve excellent mechanical properties in heat-treatable Al alloys. Usually, the homogenization temperature for common heat-treatable Al alloys falls in the temperature range for Al_3Sc precipitation [1,14], Al_3Sc dispersoids are expected to form during the homogenization treatment if the addition of Sc is enough. The Al_3Sc dispersoids can be survived or partially dissolved to become solute atoms in subsequent solution treatment, depending on the solution temperature. The existing forms of added Sc, either Al_3Sc dispersoids or Sc solute atoms, should have different influences on the final aging response. Of special interest to note is the possible interaction between the Al_3Sc dispersoids and other precipitates. The nanoscale Al_3Sc particles have an equilibrium shape of Great Rhombicuboctahedron [14], with a total of 26 facets on the {1 0 0}, {1 1 0} and {1 1 1} planes (Fig. 1(a) and (b)). In further evolution at growth process, coarsened Al_3Sc particles still have some clear plane facets [14] (Fig. 1(a)). When the plane of these facets fits well with the habit plane of some non-spherical precipitates, such as the {1 0 0}-Al_2Cu plates in Al–Cu alloy (Fig. 1(c) and (d)), the Al_2Cu plates will have a strong interaction with the early-formed Al_3Sc dispersoids.

The purpose of present work was to examine the influence of solution treatment on the precipitation behaviors and age hardening response of Al–Cu–Sc alloy, in comparison with Sc-free one. The present results show that the solution treatment is crucial for achieving a significant strengthening effect in the heat-treatable Al alloys with Sc addition.

2. Experimental procedures

Two kinds of alloys, *i.e.*, Al–2.5 wt% Cu alloys with 0.3 wt% Sc and without Sc, were respectively melted and cast in a stream argon, by using 99.99 wt% pure Al, 99.99 wt% Cu, and Al–2.0 wt% Sc. Ingots of these alloys were homogenized at 723 K for 4 h. Specimens of 10 mm × 10 mm in size were cut from the ingots and subjected to further heat treatments. For comparison reason, solution treatment was performed at two temperatures, 793 K and 873 K, respectively for 3 h. The former temperature is within the traditional regime for solution treatment of binary Al–Cu alloys, where the Cu can be well dissolved into the α-Al while most of the Al_3Sc dispersoids will survive. The latter one is carefully selected to dissolve more Al_3Sc dispersoids as possible. The solution-treated samples were directly quenched into water at room temperature, followed by aging treatment at 523 K for various times. At this aging temperature, θ'-Al_2Cu precipitates are preferential to form while Al_3Sc particles are hard to precipitate. The maximum error of all the temperature measurements was ±1 K.

The θ'-Al_2Cu precipitates (lattice structure in Fig. 1(e)) and Al_3Sc dispersoids (lattice structure in Fig. 1(f)) were quantitatively characterized by using transmission electron microscope (TEM) and high resolution TEM (HRTEM). TEM foils were prepared following standard electro-polishing techniques for Al alloys. Quantitative measures of the number density, size (radius for the Al_3Sc dispersoids and length/thickness for the θ' precipitates) were reported as average values of more than 200 measurements that were carried out on at least five different local areas from center to surface layer of the samples. Volume fraction of the particles was determined by using corrected projection method [27,28]. Details about the microstructural measurements can be referred to previous publications [27,29–31].

Vickers microhardness was measured on polished samples and each data point was come from an average of at least ten measurements made on several grains.

Table 1
Mean size, number density and volume fraction of Al_3Sc dispersoids after different heat treatments.

Heat treatment	r_d^{av} (nm)	N_d (10^{18} m^{-3})	f_d (10^{-2})
As-homogenized	8 ± 2	610 ± 50	0.12 ± 0.02
Solution-treated at 793 K	49 ± 6	2.3 ± 0.4	0.11 ± 0.04
Solution-treated at 793 K	89 ± 10	0.3 ± 0.1	0.01 ± 0.004

3. Results and discussions

3.1. Effect of solution treatment on the Al_3Sc dispersoids

Fig. 2(a) shows microstructure of the Sc-added Al–Cu alloy after homogenization treatment. A larger number of coherent Al_3Sc dispersoids are uniformly distributed in the matrix. The Al_3Sc particles have clear facets on the {1 0 0} planes (Fig. 1(a)). This is similar to what observed by Marquis and Seidman [14] in Al–0.3 wt% Sc alloy. Statistical analyses reveal that the Al_3Sc dispersoids have an average radius of about 8 nm with a very narrow size distribution (Fig. 2(d)). After solute-treated at 793 K, a number of Al_3Sc dispersoids can still be seen (Fig. 2(b)). But the dispersoids have coarsened to an average radius of about 49 nm, with a much wide size range from 8 nm to 75 nm (Fig. 2(e)). After solute-treated at 873 K, however, both the number density and the volume fraction of Al_3Sc dispersoids are remarkably reduced (Fig. 2(c) and Table 1), indicative of the dissolution of most Al_3Sc dispersoids. These results show that the existence of Al_3Sc dispersoids can be controlled to some extent by changing the solution temperature. Lower is the solution temperature, more is the Al_3Sc dispersoids revived. Increasing the solution temperature, some Al_3Sc dispersoids will be dissolved and Sc will predominantly exist as solute atoms. Measurements on the parameters (mean radius r_d^{av}, number density N_d, and volume fraction f_d) of the Al_3Sc dispersoids at different solution treatments are summarized in Table 1 for comparison.

3.2. Precipitation in 793 K-solution-treated samples

During the aging treatment of Al–Cu–Sc alloy solution-treated at 793 K, an unusual precipitation behavior was also observed besides the homogeneous precipitation in matrix, see Fig. 3(a). A series of plate-like precipitates were arranged to form an enclosed local region, as indicated by white arrows. Composition and structural analyses [32] showed that the "enclosed" central parts were Al_3Sc and the surrounding plate-like precipitates were θ'-Al_2Cu, respectively. The Al_3Sc phases are actually the Al_3Sc dispersoids existed before the aging treatment and the θ'-Al_2Cu plates are precipitated directly on the Al_3Sc dispersoids during the aging treatment. This is a typical heterogeneous precipitation, *i.e.*, precipitation of θ'-Al_2Cu plates on interface between the Al_3Sc dispersoids and matrix. The orientation relationship between θ'-Al_2Cu precipitate and Al_3Sc

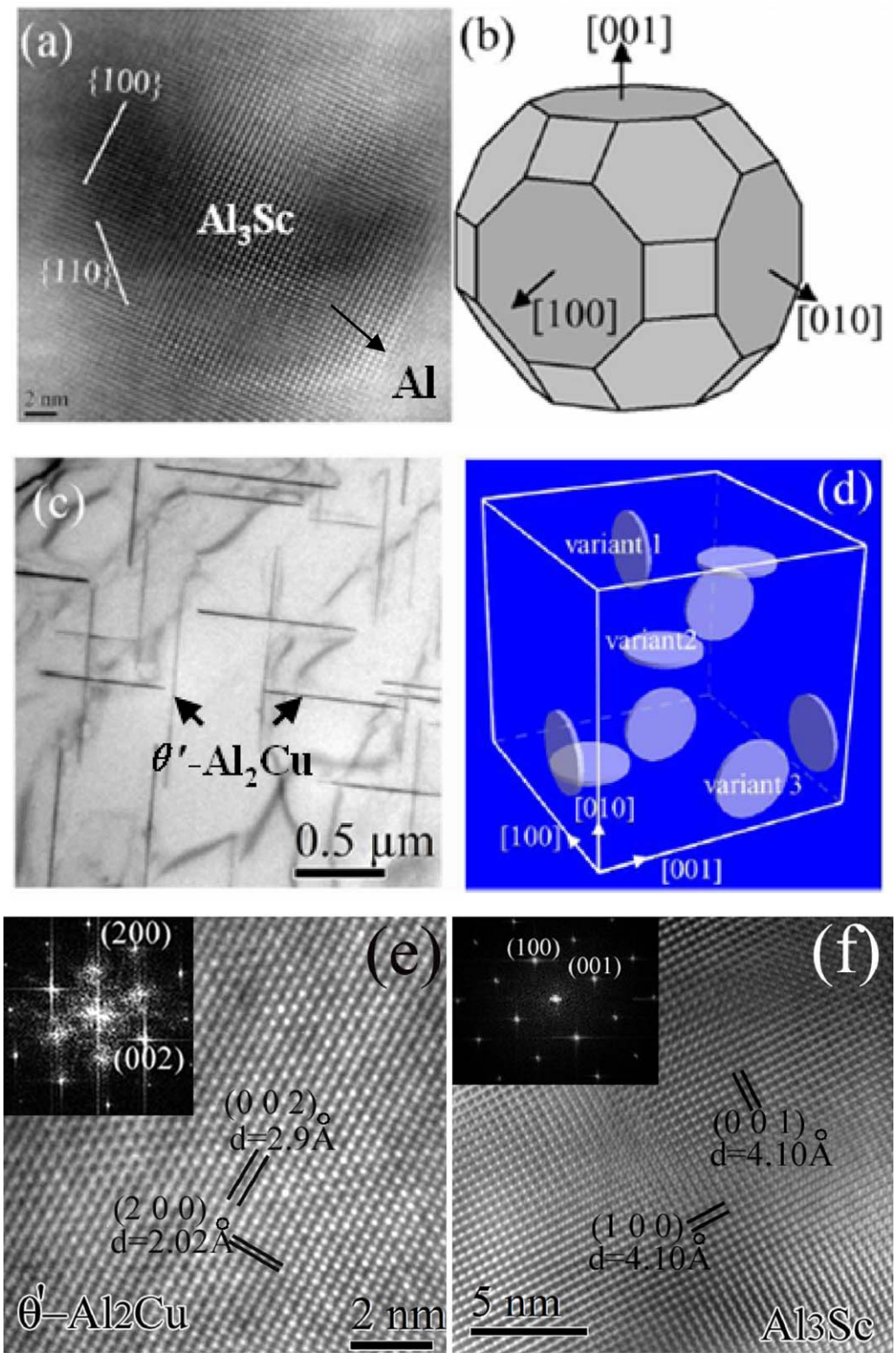

Fig. 1. (a) Representative HRTEM image showing the morphology of Al_3Sc dispersoid in the present as-homogenized Al–Cu–Sc alloy where the {1 0 0} facets are clear. Interface between the Al_3Sc dispersoid and Al matrix is indicated by arrow. (b) Wulff's construction of the Al_3Sc nanoparticle morphology at 0 K based on first-principle calculations [14]. (c) Representative TEM image showing the distribution of θ'-Al_2Cu precipitates in Al–Cu alloy aged at 523 K for 4 h. (d) Schematic diagram illustrating the distribution of θ'-Al_2Cu precipitates in a cubic volume of the matrix. The lattice structure of θ'-Al_2Cu and Al_3Sc is indexed in (e) and (f), respectively.

dispersoids can be determined as [32]: (0 0 1) θ'-Al_2Cu//{0 0 1} Al_3Sc and [0 1 0] (or [1 0 0]) θ'-Al_2Cu//⟨0 0 1⟩ Al_3Sc. Fig. 3(b) is a representative HRTEM image showing the interface between the θ'-Al_2Cu precipitate and the Al_3Sc dispersoids, from which one can see the interface is coherent/semi-coherent. The orientation relationship between the θ'-Al_2Cu precipitate and the Al matrix is remained the same as (0 0 1) θ'-Al_2Cu//(0 0 1) Al and [1 0 0] θ'-Al_2Cu//[1 0 0] Al. Sketches in Fig. 3(c) and (d) schematically illustrate the

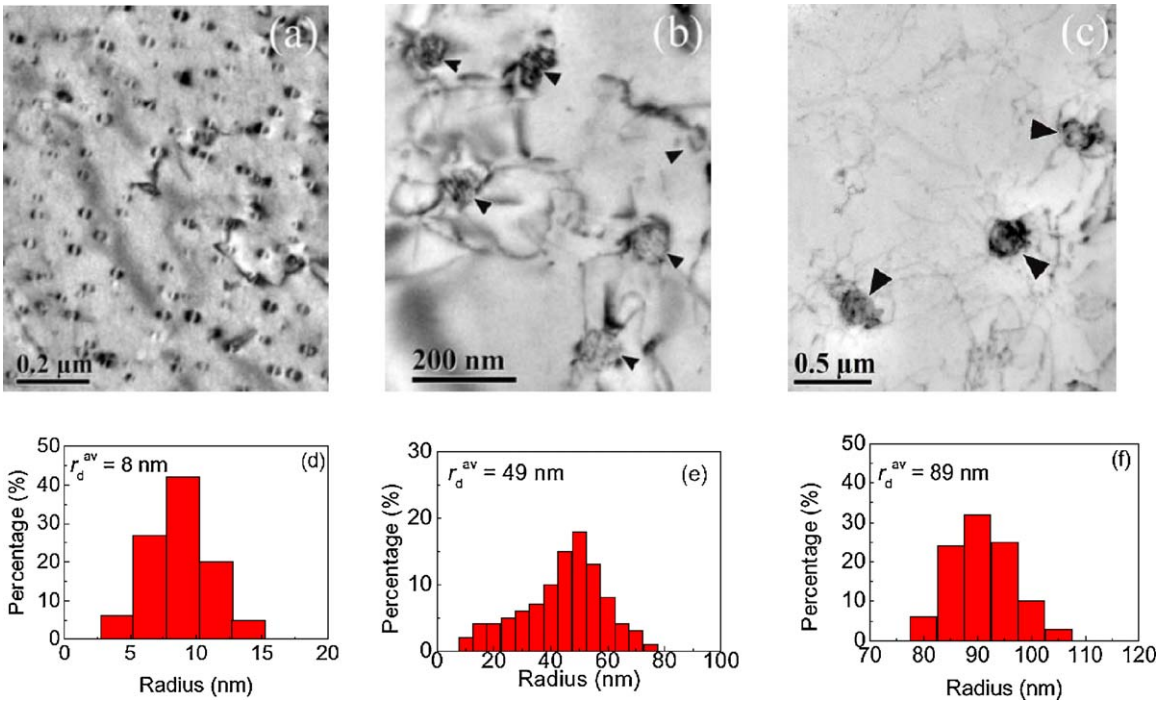

Fig. 2. Representative TEM images of Al_3Sc dispersoid in the Al–Cu–Sc alloy after (a) homogenized at 723 K for 4 h, (b) solutionized at 793 K for 3 h, and (c) solutionized at 873 K for 3 h. The corresponding measurements on size distribution of Al_3Sc dispersoid are given in (d)–(f), respectively.

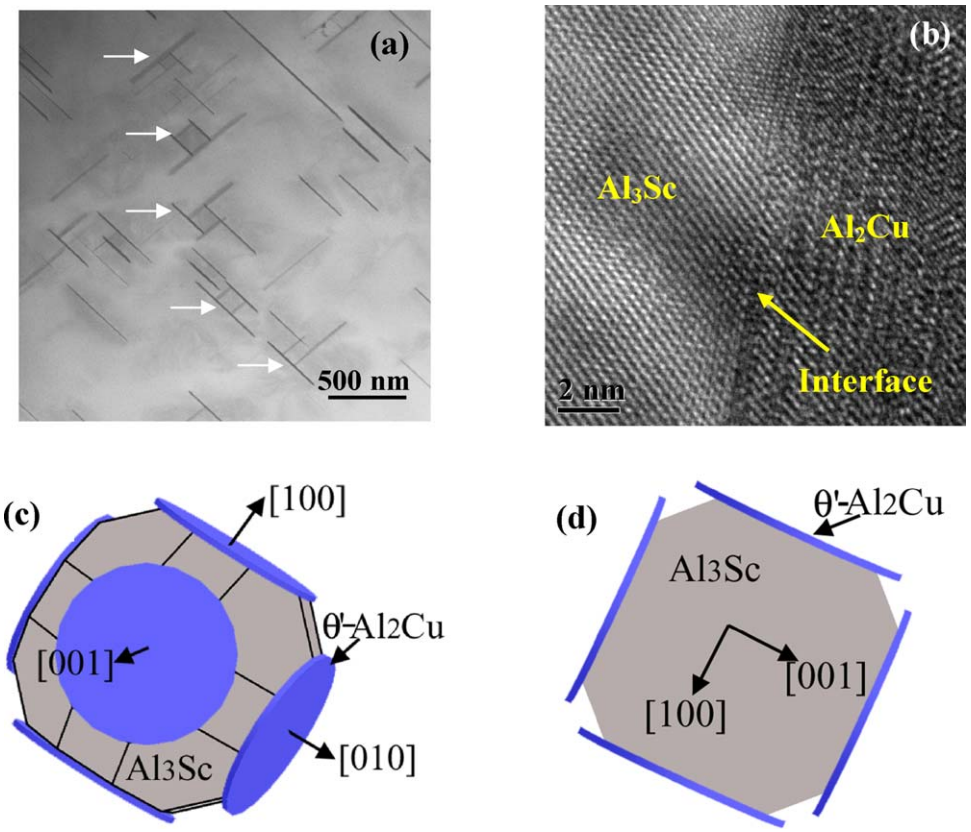

Fig. 3. (a) Representative TEM image of the 793 K-solution-treated Al–Cu–Sc alloy aged for 10 h, where the "enclosed" groups or the heterogeneous precipitations are indicated by arrows. (b) is a HRTEM image showing the interface between the Al_3Sc dispersoid and the θ'-Al_2Cu plate within the "enclosed" groups. (c) and (d) schematically illustrate the heterogeneous precipitation of θ'-Al_2Cu plates directly on the Al_3Sc dispersoid from a three-dimension and ⟨0 1 0⟩ direction-projection view, respectively.

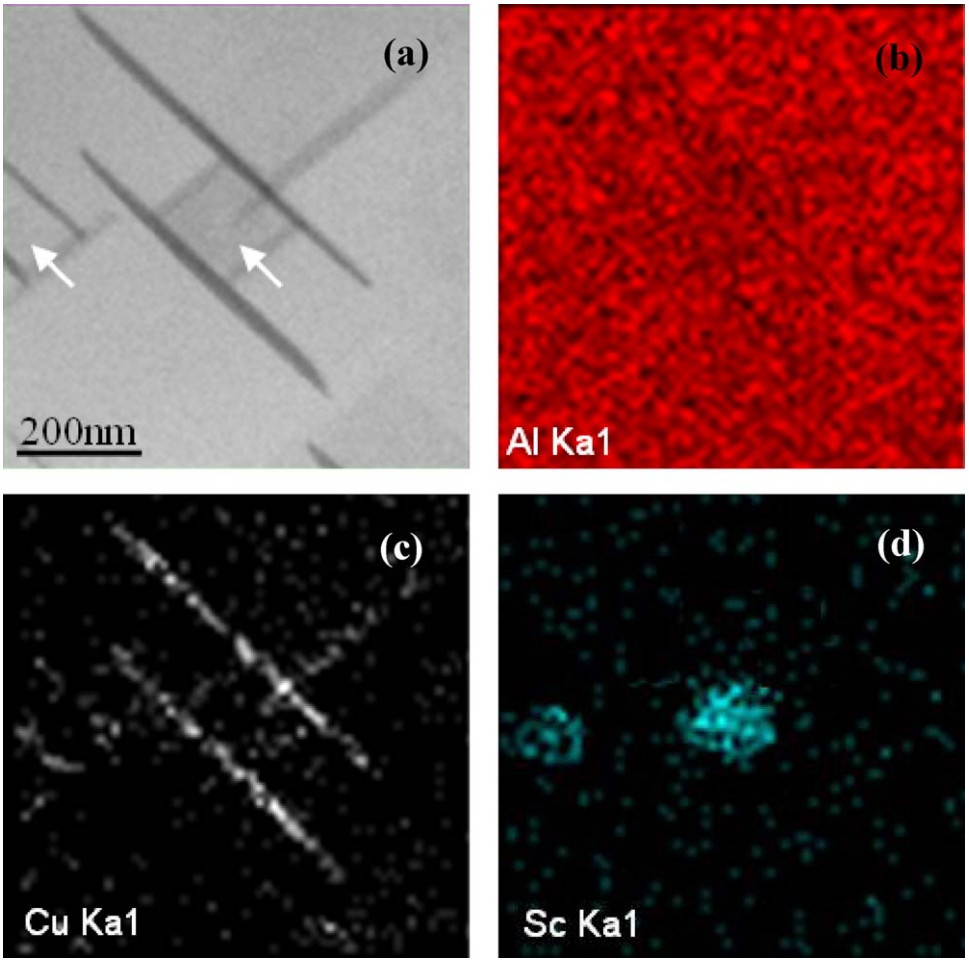

Fig. 4. (a) Representative TEM image of "enclosed" groups in the 793 K-solution-treated Al–Cu–Sc alloy aged for 16 h. The corresponding composition mapping of Al, Cu and Sc is shown in (b), (c) and (d), respectively.

heterogeneous precipitation of θ'-Al_2Cu plates directly on the {1 0 0} plane of Al_3Sc dispersoid from a three-dimension and ⟨0 1 0⟩ direction-projection view, respectively. Fig. 4 further shows the composition mapping of some representative "enclosed" groups. The centers are rich in Sc (Fig. 4(d)) and the surrounding plates are rich in Cu (Fig. 4(c)), agreeing well with above analyses.

Interestingly, the heterogeneous precipitation was only observed on Al_3Sc dispersoids with radius larger than about 20 nm, which is related to the coherency loss of the dispersoids. Previous investigations [1,14,33] showed that the nanoscaled Al_3Sc particles will loss coherency when grow to larger size. The critical radius for coherency loss was reported to between 8 and 20 nm [14,33]. In present 793 K-solution-treated Al–Cu–Sc alloy where the Al_3Sc dispersoids have a wide size range from 8 nm to 75 nm, coherent, semi-coherent, and incoherent Al_3Sc particles are coexistent (Fig. 5(a) and (b)). Generally, particle coherency can be simply judged from Ashby and Brown (AB) contrast, for which details can be referred to Iwamura and Miura's paper [33] on analyzing the coherency less of Al_3Sc particles. The AB contrast appears around a spherical coherent particle in bright field images under the just Bragg condition. So-called no-contrast line appears in normal direction to the g vector. Loss of spherical strain caused by the introduction of interfacial dislocations can be detected by the irregularity of the no-contrast line. In this paper, we judge the coherency of Al_3Sc dispersoids by using the same approach. HRTEM images typically showing the interface between coherent, semi-coherent, and incoherent Al_3Sc dispersoids with Al matrix are respectively given in Figs. 5(c), 1(a), and 5(d), where the interface is indicated by arrow. The critical radius for coherent/semi-coherent transition is determined about 20 nm, in broad agreement with previous reports. When the dispersoid coherency is lost, interfacial dislocations are formed (Fig. 5(b)), for which the driving force mainly arises from the elastic energy caused by the lattice misfit. The increase in interfacial energy by introduction of dislocations makes the Al_3Sc particle interface thermodynamically favorite for the nucleation of θ' precipitates. From the crystallography view, the broad faces of θ' precipitates have a crystal structure compatible to the Al_3Sc (lattice misfit of only about 0.012). These ensure that the θ' precipitates are preferential to nucleate on the interface between the Al_3Sc dispersoids and matrix, and grow to form "enclosed" groups.

Precipitation behaviors were compared between Sc-free and Sc-containing Al–Cu alloys. Fig. 6(a)–(d) shows some representative microstructure images for the two alloys aged at different times, respectively. Homogeneous and heterogeneous precipitations of the θ' precipitates are simultaneous in the Sc-containing Al–Cu alloys (Fig. 6(c) and (d)), while only homogeneous precipitation is observed in the Sc-free Al–Cu alloys (Fig. 6(a) and (b)). Measurements results (Fig. 6(e) and (f)) reveal that the homogeneous precipitation was remarkably suppressed after the Sc addition. Compared with their Sc-free counterparts, the Sc-containing Al–Cu alloys exhibit slower growth rate, lower number density, and less volume fraction in the homogeneous precipitation of θ' plates. But aspect ratio (A) of the homogeneously precipitated θ' plates shows

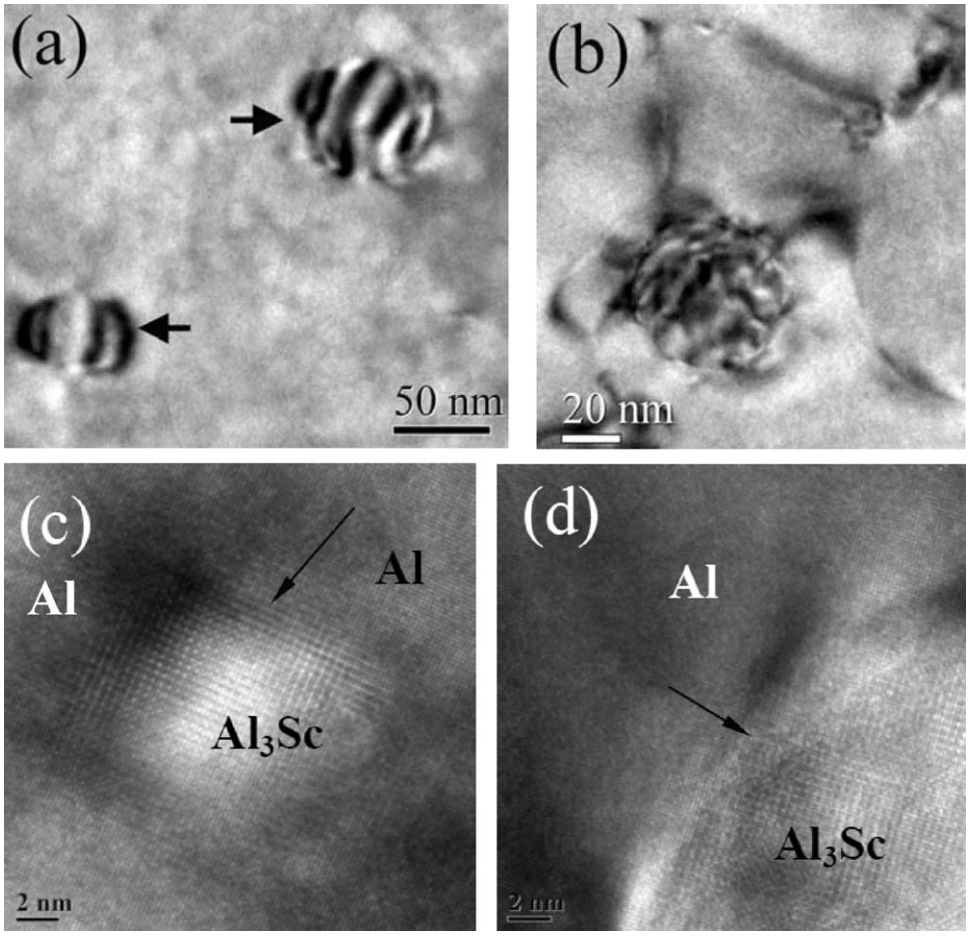

Fig. 5. Co-existence of coherent (left bottom in (a)), semi-coherent (right top in (a)), and incoherent (b) Al_3Sc dispersoids in the 793 K-solution-treated Al–Cu–Sc alloy. Interfacial dislocations can be clearly observed in (b). (c) and (d) are the HRTEM images showing the interface (indicated by arrow) between the coherent and incoherent Al_3Sc with Al matrix, respectively.

no visible change before and after the Sc addition. The suppression of homogeneous precipitation in the Sc-containing Al–Cu alloys is attributed to competition from heterogeneous precipitation of "enclosed" groups, which consumed a part of Cu solutes and hence decreased the solute atoms available for homogeneous precipitation.

The heterogeneously precipitated θ' plates were found to grow in a much slower rate ($\sim$70 nm/h$^{1/2}$), two times less than that of the homogeneously precipitated θ' plates (Fig. 6(e)). This means that the growth of heterogeneous θ' precipitates is strongly inhibited in present case. Insufficient solute supply is responsible for this inhibition. Within the "enclosed" groups, the heterogeneous θ' precipitates have a high local number density. Simultaneous growth of these precipitates requires surrounding matrix to provide much more solute atoms. The diffusive fields of adjacent growing precipitates are apt to overlap. These greatly limit the free growth of the heterogeneous precipitates, resulting in much slow growth rate as well as low aspect ratio (Fig. 6(f)). Number density of the heterogeneous θ' precipitates is almost independent of aging time (Fig. 6(g)). This indicates that heterogeneous θ' plates are very ready to precipitate on the Al_3Sc dispersoids and can quickly attain a saturated density at short aging durations.

Brief summary of precipitation behaviors in the 793 K-solution-treated Sc-added Al–Cu alloys is that the existence of Al_3Sc dispersoids promotes the heterogeneous precipitation of θ' plates and concomitantly suppresses the homogeneous precipitation.

3.3. Precipitation in 873 K-solution-treated samples

In the Al–Cu–Sc alloys solution-treated at 873 K, however, most of the Al_3Sc dispersoids have been dissolved and Sc is existed predominantly as solute atoms. During subsequent aging treatment, heterogeneous precipitation on the Al_3Sc dispersoids is seldom observed. On the contrary, the uniform precipitation of θ' plates was significantly improved. See the comparison in microstructure between the Al–Cu and Al–Cu–Sc alloys aged at different times (Fig. 7(a) and (b) *vs.* (c) and (d)) and the comparison in precipitate parameters between the Al–Cu–Sc alloys solution-treated at 793 K and 873 K (Fig. 6(e) and (g) *vs.* Fig. 7(e) and (g)), respectively, the Sc addition as solute atoms remarkably increases the number density (Fig. 7(g)) while reduces the size and aspect ratio of the θ' precipitates (Fig. 7(e) and (f)).

The effect of Sc solute atoms on uniform precipitation of θ' plates can be interpreted in term of two major factors, *i.e.*, solute–solute interaction and solute–vacancy interaction. Refer to the calculated enthalpy of solute in infinite dilution [34], the negative enthalpy value ($\sim$−115 kJ/mol) of Sc–Cu means that Sc–Cu pair is ready to form thermodynamically. The interaction of solute–vacancy is determined by the solute–vacancy binding energy. The Sc–vacancy binding energy in Al has been experimentally measured [35] to have a value (0.35 eV), which is much higher than the Cu–vacancy binding energy (<0.10 eV [36]). The high Sc–vacancy interaction contributes to the formation of Sc–vacancy pairs which would be arranged in clusters with vacancies and multiple solute atoms. The

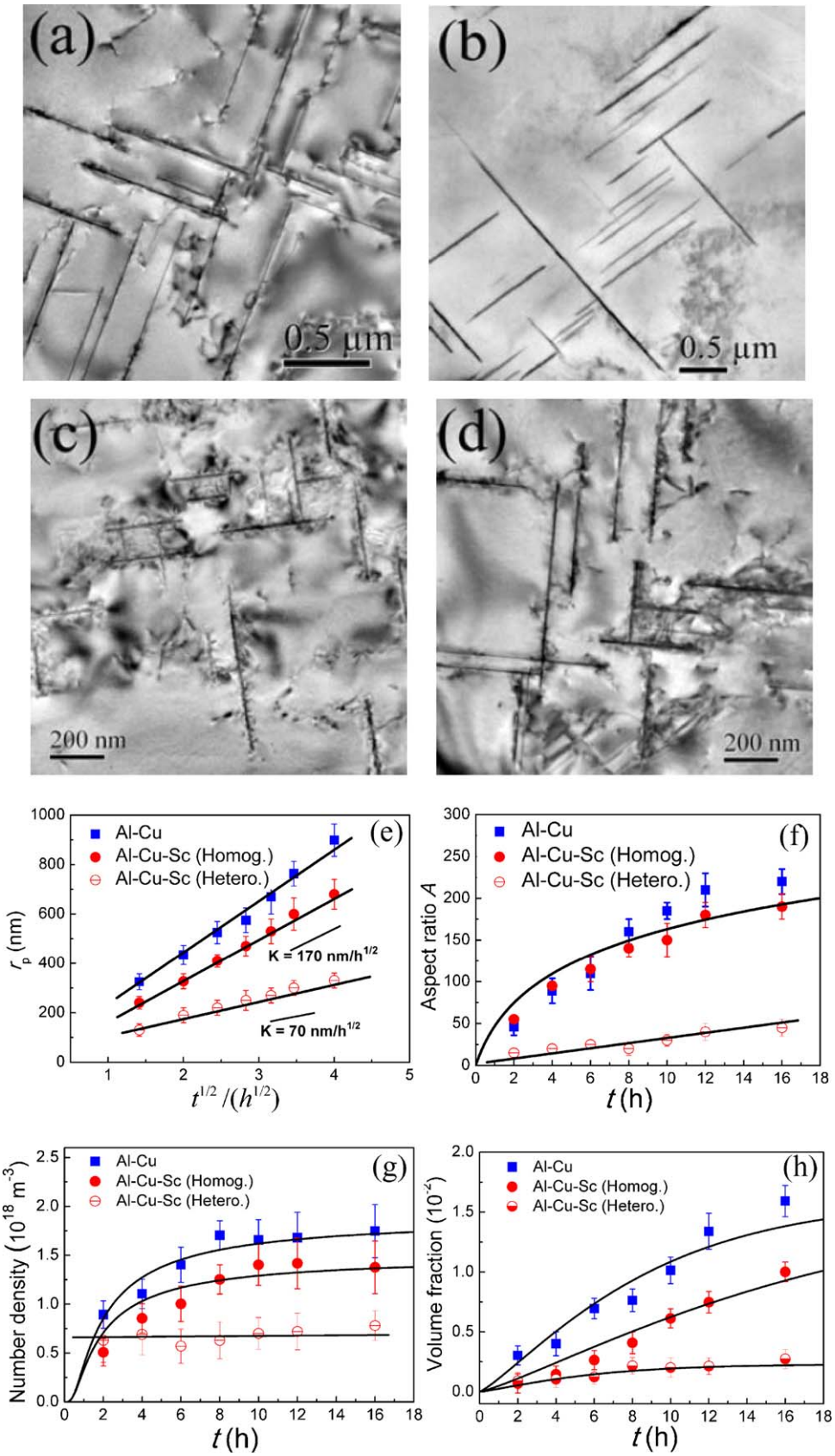

Fig. 6. Representative TEM image of the 793 K-solution-treated Al–Cu alloy aged at 523 K for 8 h (a) and 14 h (b), and the Al–Cu–Sc alloy aged at 523 K for 8 h (c) and 14 h (d). Measurements on size (e), aspect ratio (f), number density (g), and volume fraction (h) are quantitatively given for the two alloys as a function of aging time. Note that homogeneous and heterogeneous precipitations are separated in the Al–Cu–Sc alloy.

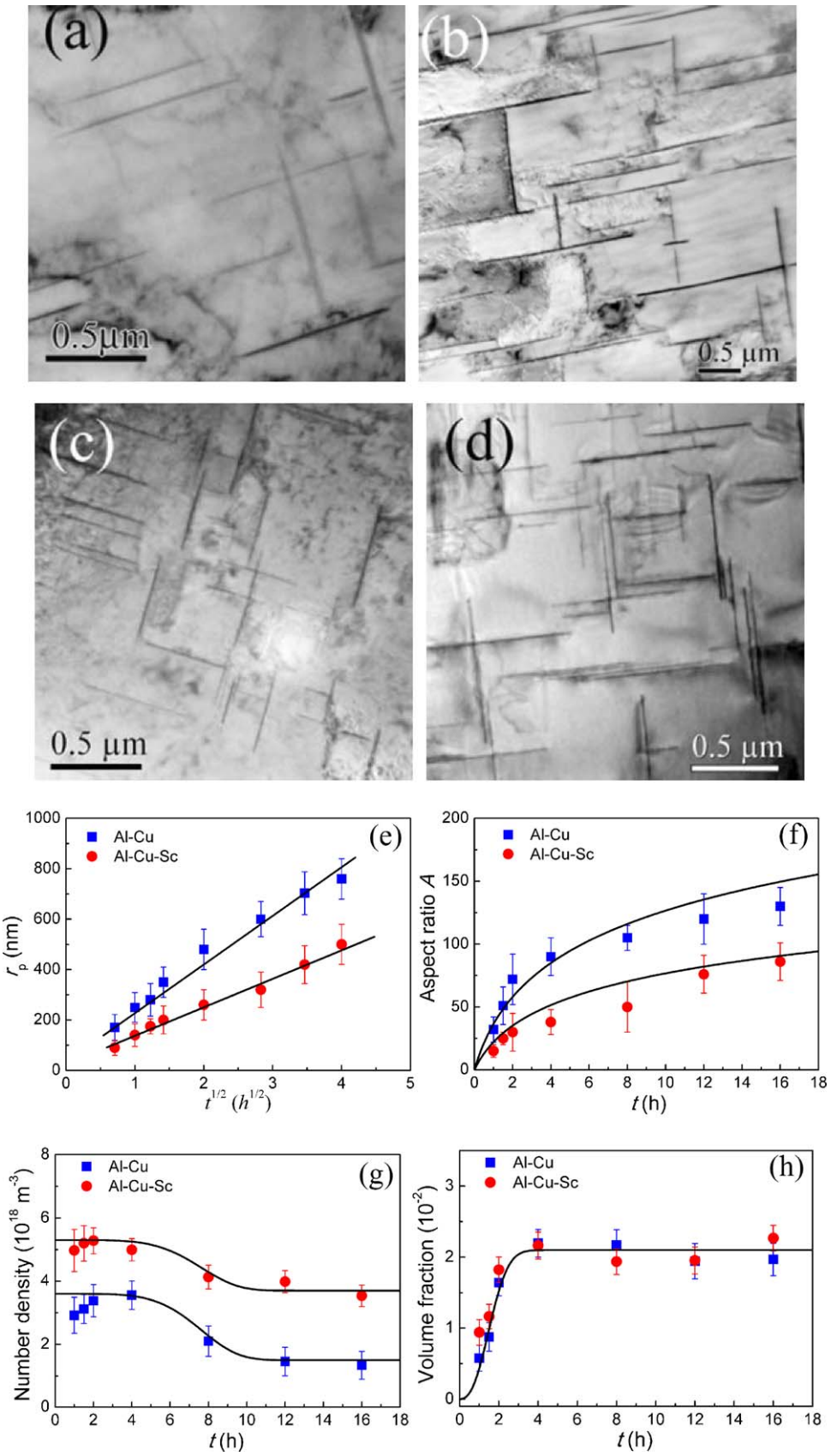

Fig. 7. Representative TEM image of the 873 K-solution-treated Al–Cu alloy aged at 523 K for 2 h (a) and 8 h (b), and the Al–Cu–Sc alloy aged at 523 K for 2 h (c) and 8 h (d). Measurements on size (e), aspect ratio (f), number density (g), and volume fraction (h) are quantitatively given for the two alloys as a function of aging time.

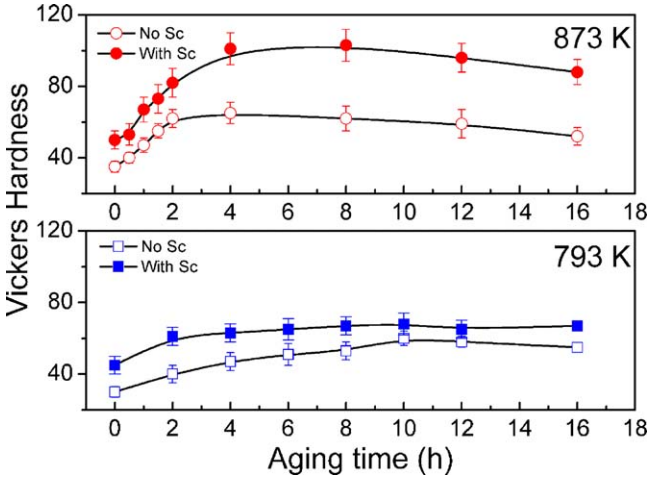

Fig. 8. Variation of Vickers hardness with aging time (t) for the Al–Cu alloy and Al–Cu–Sc alloy solution-treated at 793 K and 873 K, respectively.

strong Sc–Cu interaction may encourage Sc–vacancy clusters to seize Cu atoms. The Cu/Sc/vacancy complex clusters are expected to act as preferential nucleation sites for precipitates and resultantly accelerate the formation of fine and high density precipitates [37,38]. This can explain why the precipitation of θ' precipitates has been improved in the presence of Sc solute atoms (Fig. 6(g)), similar to the case in Al–Cu-based alloys promoted by Mg microalloying element [37,38]. The retardation in precipitation growth is related to the enhanced nucleation. Because more plates grow simultaneously, the solute atoms will be in lack supply and the diffusion fields are also easy to overlap, which inhibits the lengthening of θ' plates and results in reduced radius (Fig. 7(e)) and aspect ratio (Fig. 7(f)).

In careful HRTEM examinations, we did not observe the precipitation of nanosized Al_3Sc precipitates during the aging treatment. The main reason for this absence is that the aging temperature of 523 K is somewhat low (generally larger than 573 K in previous reports [13–17]), which limits the diffusion of Sc atoms. Another possible reason is that the presence of Cu suppresses the precipitation of Al_3Sc. Copper in solid solution decreases the lattice parameter of the Al matrix. It is expected that the misfit between the Al matrix and Al_3Sc should be higher in Al–Cu–Sc alloys compared to Al–Sc alloys [1]. We should note that the suppression in Al_3Sc precipitation is not related to the formation of W-phase (Al, Cu, Sc), because no W-phase was observed in the current Al–Cu–Sc alloys.

Brief summary of precipitation behaviors in the 873 K-solution-treated Sc-added Al–Cu alloy is that the introduction of Sc solute atoms promotes the homogeneous precipitation of θ' plates by enhancing the precipitate nucleation and reducing the precipitate growth.

3.4. Vickers hardness

Vickers hardness (Hv) is compared between the Al–Cu alloys with and without Sc addition. When the solution temperature is 793 K, the Sc addition causes very limited increase (about 15%) in Vickers hardness, see Fig. 8, indicative of a weak effect. In the 873 K-solution-treated Al–Cu–Sc alloy, however, the peak-aged Vickers hardness is increased by about 90% compared to its Sc-free counterparts. This significant increase can be possibly explained by two contributions: (i) the strengthening effect directly from Sc-based precipitates or clusters, and (ii) the improved strengthening effect from uniform distribution of θ' precipitates promoted by the Sc atoms. For clarity, we also measured the Vickers hardness of Al–0.3 wt% Sc alloy (without Cu) that was heat-treated strictly following the 873 K-solution-treated Al–Cu–Sc alloy, and found only slight change in Vickers hardness during the 523 K-aging treatment (from $Hv = 22 \pm 3$ at 0 h to $Hv = 28 \pm 5$ at 8 h). This means that the first contribution is actually unimportant, which is agreeable with the microstructural observation that no Al_3Sc precipitates were formed during the aging treatment. The second contribution is then believed to be responsible for the significant promotion in the age hardening response. As mentioned before, experimental results have verified that the presence of Sc atoms promotes the uniform precipitation of θ' plates by increasing the number density and decreasing the size. The solution treatment, which controls the existing form of added Sc, is thus crucial for achieving the promotion effect of Sc addition in the Al–Cu alloys.

The time required to attain peak aging is reduced by increasing the solution temperature from 793 K to 873 K, regardless of Sc-addition or not. Vacancies play an important role in the precipitation of θ' plates. The equilibrium concentration of vacancies is closely dependent on the temperature. The higher is the solution temperature, the more are the equilibrium vacancies. When quenched from 873 K solution, the vacancies retained in the solid solution are relatively high, which will facilitate the precipitation in aging treatment.

3.5. Modeling of the age hardening response

It has been revealed from Fig. 8 that the presence of Sc solute atoms causes a significant improvement in age hardening in the 873 K-solution-treated Al–Cu–Sc alloy. While in the 793 K-solution-treated Al–Cu–Sc alloy where Sc is existed as Al_3Sc dispersoids, the hardness increment during aging treatment is only slightly higher than that in its Sc-free alloy. This difference is of course resulted from the different evolution of θ' precipitates affected by the Al_3Sc dispersoids and by the Sc solute atoms. To understand the age hardening effect with respect to precipitation behavior, a quantitative relationship is required to relate the macroscopic hardness/strength increment to the microstructural parameters of the precipitates.

The increment $\Delta\tau$ in critical resolved shear stress needed to bow a dislocation between particles is generally expressed by [39–41]

$$\Delta\tau = \frac{Gb}{2\pi\sqrt{1-\nu}} \cdot \frac{1}{\lambda} \cdot \ln\left(\frac{r_0}{r_i}\right), \tag{1}$$

where r_0 and r_i are outer and inner cut-off radii respectively for matrix dislocations, λ is the effective planar inter-particle spacing in the slip plane. For randomly distributed spherical precipitates, λ is dependent on the two variants of size (r_p) and volume fraction (f_p) of precipitates

$$\lambda \sim \frac{r_p}{\sqrt{f_p}}. \tag{2}$$

Increasing f_p and/or reducing r_p are the two well-known strategies for increasing the strengthening increment from shear-resistant spherical precipitates. But for plate-like precipitates formed on habit planes, λ is complicated by the presence of two additional variants, *i.e.*, aspect ratio and orientation. A modified version on λ, termed λ_{ave}, has been recently developed [42–44] for the $\{1\,0\,0\}_\alpha$-θ' precipitates in Al–Cu alloys

$$\lambda_{ave} = \sqrt{\frac{\sqrt{3}}{2}} \frac{1}{\sqrt{2\,\sin\theta \cdot N \cdot r_p}} - \frac{\pi r_p}{4} - \frac{\sqrt{3} r_p}{A \cdot \sin\,\theta}, \tag{3}$$

with $\theta = 54.74^\circ$ being the dihedral angle between the plate and the $\{1\,1\,1\}_\alpha$ slip plane. Compared with λ in Eq. (2), λ_{ave} is a more comprehensive parameter that combines the size, number density, and aspect ratio of the plate-shaped precipitates. Based on above

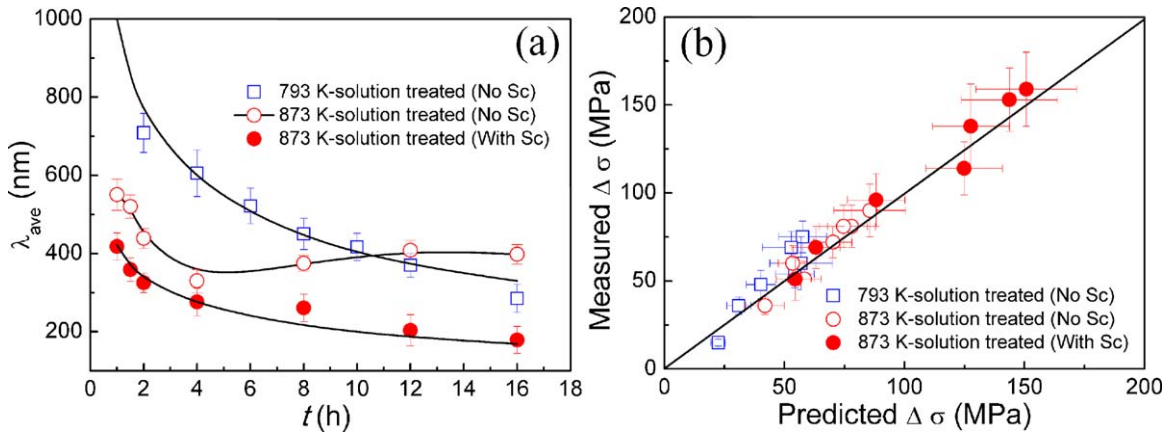

Fig. 9. (a) t-dependent effective planar inter-particle spacing (λ_{eff}) for the 793 K-solution-treated Al–Cu and Al–Cu–Sc alloys and the 873 K-solution-treated Al–Cu–Sc alloy. (b) Comparison between the predictions and the experimental results on the increment in strength ($\Delta\sigma$) during the aging treatment.

equation, the increment ($\Delta\sigma$) in strength caused by θ' precipitates is

$$\Delta\sigma = \frac{MGb}{2\pi\sqrt{1-\nu}} \cdot \frac{1}{\lambda_{ave}} \cdot \ln\left(\frac{r_0}{r_i}\right), \quad (4)$$

where M is the Taylor factor.

Obviously, Eq. (4) works only when one single kind of precipitates is homogeneously distributed. In the present work, predominant homogeneous precipitation of θ' plates is observed in Al–Cu alloys (solution-treated at both 793 K and 873 K) and Al–Cu–Sc alloy solution-treated at 873 K. Therefore, λ_{ave} and $\Delta\sigma$ are calculated for the three alloys by using the measurements of N, r_p, and A (Figs. 6(e)–(g) and 7(e)–(g)), respectively and some parameter values listed in Table 2. Fig. 9(a) is the variation of λ_{ave} with aging time for the three alloys and Fig. 9(b) shows the comparison between the predicted $\Delta\sigma$ and experimental $\Delta\sigma$ (=3 × ΔHv [46]). It is revealed that the prediction on strength increment is in good agreement with the experimental, indicating that λ_{ave} given in Eq. (3) is an effective parameter for representing the combined effect of multiple variants of plate-like precipitates.

From Fig. 9(a), one can find that the precipitates in 873 K-solution-treated Al–Cu–Sc alloy have λ_{ave} much narrower than their Sc-free counterpart. The main reason is that the Sc addition as solute atoms promotes the nucleation of θ' plates and increases the number density (see Fig. 7(g)). When the precipitates grow to large size, the effective planar inter-particle spacing in the slip plane will be noticeably reduced, making dislocations hard to pass through. As a result, a significant age hardening response is achieved.

In the Al–Cu–Sc alloy solution-treated at 793 K, however, the age hardening response is slight in spite of the co-existence of multiple strengthening obstacles, *i.e.*, the homogeneous θ' precipitates and heterogeneous θ' + Al_3Sc dispersoids groups. As discussed before, the heterogeneous precipitation of θ' precipitates consumes a large number of Cu solute atoms and hence suppresses the homogeneous precipitation of θ' precipitates. The low number density shown in Fig. 6(g) hints a wider inter-particle spacing and an easier way for dislocations to pass through the obstacles.

Finally, it should be pointed out that the effective inter-particle spacing of the "enclosed" θ'-plate + Al_3Sc dispersoid groups is much hard to quantitatively describe, due to the complicated geometry of the groups. So the hardness/strength increment in 793 K-solution-treated Al–Cu–Sc alloy was not modeled here. These groups, although contributing less to the strength, were found to have remarkable effect on the high-temperature mechanical properties of the Al–Cu–Sc alloys, which will be discussed elsewhere.

Table 2
Summary of some parameters and their values used for calculations.

Parameter	Value or expression	Ref.
b (nm)	0.286	[45]
M	3.1	[45]
G (GPa)	28	[45]

4. Conclusions

(1) The Sc addition in Al–Cu alloys as Sc solute atoms produces a significant strengthening effect by promoting the uniform precipitation of θ'-Al_2Cu plates and increasing the peak-aged hardening response by about 90%. The promotion effect by Sc solute atoms can be interpreted in terms of the solute–vacancy and solute–solute interactions.

(2) The achievement of significant strengthening effect with Sc addition is closely dependent on the solution treatment. Because Al_3Sc dispersoids were firstly formed in homogenization treatment, the solution temperature should be high enough (e.g., 873 K in present experiment) to dissolve most of the Al_3Sc dispersoids. Otherwise, the Al_3Sc dispersoids will induce heterogeneous precipitation of θ'-Al_2Cu plates, suppressing the homogeneous precipitation and reducing the age hardening response.

(3) In the Al–Cu–Sc alloy where Sc is predominantly existed as solute atoms, the remarkable age hardening effect is quantitatively described with regard to the reduced effective inter-particle spacing that represents a characteristic parameter of the plate-shaped precipitates.

Acknowledgements

This work was supported by the National Basic Research Program of China (Grant No. 2010CB631003 and 2012CB619604) and the National Natural Science Foundation (51171142). This work was also supported by the 111 Project of China under Grant No. B06025 and the Fundamental Research Funds for the Central Universities.

References

[1] J. Røyset, N. Ryum, Int. Mater. Rev. 50 (2005) 19.
[2] M.J. Jones, F.J. Humphreys, Acta Mater. 51 (2003) 2149.
[3] M. Ferry, N. Burhan, Acta Mater. 55 (2007) 3479.
[4] J.S. Vetrano, S.M. Bruemmer, L.M. Pawlowski, I.M. Robertson, Mater. Sci. Eng. A 238 (1997) 101.
[5] M.E. Drits, S.G. Pavlenko, L.S. Toropova, Y.G. Bukov, L.B. Ber, Sov. Phys. Dokl. 26 (1981) 344.

[6] C.B. Fuller, D.N. Seidman, Acta Mater. 53 (2005) 5415.
[7] B. Forbord, H. Hallem, J. Røyset, K. Marthinsen, Mater. Sci. Eng. A 475 (2008) 241.
[8] J.D. Robson, Acta Mater. 52 (2004) 1409.
[9] E. Clouet, L. Laé, T. Épicier, W. Lefebvre, M. Nastar, A. Deschamps, Nat. Mater. 5 (2006) 482.
[10] K.E. Knipling, R.A. Karnesky, C.P. Lee, D.C. Dunand, D.N. Seidman, Acta Mater. 58 (2010) 5184.
[11] H.H. Jo, S.I. Fujikawa, Mater. Sci. Eng. A 171 (1993) 151.
[12] M.Y. Drits, L.B. Ber, Y.G. Bykov, L.S. Toropova, G.K. Anastaseva, Phys. Met. Metall. 57 (1984) 118.
[13] G.M. Novotny, A.J. Ardell, Mater. Sci. Eng. A 318 (2001) 144.
[14] E.A. Marquis, D.N. Seidman, Acta Mater. 49 (2001) 1909.
[15] J.D. Robson, M.J. Jones, P.B. Pragnell, Acta Mater. 51 (2003) 1453.
[16] D.N. Seidman, E.A. Marquis, D.C. Dunand, Acta Mater. 50 (2002) 4021.
[17] F. Fazeli, W.J. Poole, C.W. Sinclair, Acta Mater. 56 (2008) 1909.
[18] J. Røyset, N. Ryum, D. Bettella, A. Tocco, Z.H. Jia, J.K. Solberg, O. Reiso, Mater. Sci. Eng. A 483 (2008) 175.
[19] M.L. Kharakterova, D.G. Eskin, L.S. Toropova, Acta Metall. Mater. 42 (1994) 2285.
[20] M. Nakayama, Y. Miura, Proc. 4th Int. Conf. on Aluminum Alloys, vol. I, Atlanta, GA, USA, 1994, p. 538.
[21] Z.G. Chen, Z.Q. Zheng., Scripta Mater. 50 (2004) 1067.
[22] V.I. Elagin, V.V. Zakharov, T.D. Rostova, Met. Sci. Heat Treat. 36 (1999) 375.
[23] Y.L. Wu, F.H. Froes, C. Li, A. Alvarez, Metall. Mater. Trans. 30A (1999) 1017.
[24] C.H. Joh, K. Yamada, Y. Miura, Mater. Trans. JIM 40 (1999) 439.
[25] L.I. Kaigorodova, E.I. Selnikhina, E.A. Tkachenko, O.G. Senatorova, Phys. Met. Metall. 81 (1996) 513.
[26] L.I. Kaigorodova, A.M. Drits, Y.V. Zhingel, T.V. Krymova, I.N. Fridlyander, Phys. Met. Metall. 73 (1992) 286.
[27] G. Liu, G.J. Zhang, X.D. Ding, J. Sun, K.H. Chen, Mater. Sci. Eng. A 344 (2003) 113.
[28] D.L. Gilmore, E.A. Starke Jr., Metall. Mater. Trans. 28A (1997) 1399.
[29] G. Liu, J. Sun, C.W. Nan, K.H. Chen, Acta Mater. 53 (2005) 3459.
[30] G. Liu, G.J. Zhang, R.H. Wang, W. Hu, J. Sun, K.H. Chen, Acta Mater. 55 (2007) 273.
[31] G. Liu, G.J. Zhang, X.D. Ding, J. Sun, K.H. Chen, Metall. Mater. Trans. 35A (2004) 1725.
[32] B.A. Chen, L. Pan, R.H. Wang, G. Liu, P.M. Chen, L. Xiao, J. Sun, submitted for publication.
[33] S. Iwamura, Y. Miura, Acta Mater. 52 (2004) 591.
[34] A.K. Niessen, F.R. de Boer, R. Boom, P.F. de Chatel, W.C.M. Matterns, CALPHAD 7 (1983) 51.
[35] Y. Miura, C.H. Joh, T. Katsube, Mater. Sci. Forum 331–333 (2000) 1031.
[36] R.W. Balluffi, P.S. Ho, Diffusion Metals Park, Am. Soc. Metals, OH, 1973, p. 83.
[37] T. Sato, S. Hirosawa, K. Hirose, T. Maeguchi, Metall. Mater. Trans. 34A (2003) 2745.
[38] B.P. Huang, Z.Q. Zheng, Acta Mater. 46 (1998) 4381.
[39] A.J. Ardell, Metall. Trans. A 16A (1985) 2131.
[40] E. Orowan, Symposium on Internal Stresses in Metals and Alloys, The Institute of Metals, London, 1948, p. 451.
[41] J.F. Nie, Scripta Mater. 48 (2003) 1009.
[42] J.F. Nie, B.C. Muddle, I.J. Polmear, Mater. Sci. Forum 217–222 (1996) 1257.
[43] J.F. Nie, B.C. Muddle, Acta Mater. 56 (2008) 3490.
[44] J. da Costa Teixeira, D.G. Cram, L. Bourgeois, T.J. Bastow, A.J. Hill, C.R. Hutchinson, Acta Mater. 56 (2008) 6109.
[45] F. King, Aluminum and Its Alloys, Ellis Horwood Limited, Chichester, 1987.
[46] A. Deschamps, F. Livet, A. Brechet, Acta Mater. 47 (1999) 293.